

Theoretical investigation of electron-impact ionization of W^{8+} ion

Shiping Zhang(张世平), Fangjun Zhang(张芳军), Denghong Zhang(张登红), Xiaobin Ding(丁晓彬), Jun Jiang(蒋军), Luyou Xie(颉录有), Yulong Ma(马玉龙), Maijuan Li(李麦娟), Marek Sikorski, and Chenzhong Dong(董晨钟)

Citation: Chin. Phys. B, 2024, 33 (**3**): 033401. DOI: 10.1088/1674-1056/ad1487
Journal homepage: http://cpb.iphy.ac.cn; http://iopscience.iop.org/cpb

What follows is a list of articles you may be interested in

Electron-impact ionization of W^{9+} and W^{10+}

Runjia Bao(鲍润家), Junkui Wei(魏军奎), Lei Chen(陈雷), Bowen Li(李博文), and Ximeng Chen(陈熙萌)
Chin. Phys. B, 2023, 32 (**6**): 063401. DOI: 10.1088/1674-1056/aca14d

Electron-impact ionization cross section calculations for lithium-like ions

Guo-Jie Bian(卞国杰), Jyh-Ching Chang(张稚卿), Ke-Ning Huang(黄克宁), Chen-Sheng Wu(武晨晟), Yong-Jun Cheng(程勇军), Kai Wang(王凯), and Yong Wu(吴勇)
Chin. Phys. B, 2022, 31 (**1**): 013401. DOI: 10.1088/1674-1056/ac229e

Electron-impact single ionizaiton for W^{4+} and W^{5+}

Denghong Zhang(张登红), Luyou Xie(颉录有), Jun Jiang(蒋军), Zhongwen Wu(武中文), Chenzhong Dong(董晨钟), Yinglong Shi(师应龙), Yizhi Qu(屈一至)
Chin. Phys. B, 2018, 27 (**5**): 053402. DOI: 10.1088/1674-1056/27/5/053402

Fast-electron-impact ionization process by 3p of hydrogen-like ions in Debye plasmas

Qi Yue-Ying (祁月盈), Ye Dan-Dan (叶丹丹), Wang Jian-Guo (王建国), Qu Yi-Zhi (屈一至)
Chin. Phys. B, 2015, 24 (**3**): 033403. DOI: 10.1088/1674-1056/24/3/033403

Ionization cross sections for electron scattering from metastable rare-gas atoms (Ne^* and Ar^*)

Zhang Yong-Zhi (张永志), Zhou Ya-Jun (周雅君)
Chin. Phys. B, 2013, 22 (**7**): 073402. DOI: 10.1088/1674-1056/22/7/073402

Theoretical investigation of electron-impact ionization of W^{8+} ion

Shiping Zhang(张世平), Fangjun Zhang(张芳军), Denghong Zhang(张登红)†, Xiaobin Ding(丁晓彬), Jun Jiang(蒋军), Luyou Xie(颉录有), Yulong Ma(马玉龙), Maijuan Li(李麦娟), Marek Sikorski, and Chenzhong Dong(董晨钟)

Key Laboratory of Atomic and Molecular Physics & Functional Materials of Gansu Province, College of Physics and Electronic Engineering, Northwest Normal University, Lanzhou 730070, *China*

(Received 14 November 2023; revised manuscript received 6 December 2023; accepted manuscript online 12 December 2023)

The electron-impact single ionization cross section for W^{8+} ion has been calculated using flexible atomic code, employing the level-to-level distorted-wave approximation. This calculations takes into account contributions form both direct ionization (DI) and excitation autoionization (EA). However, the theoretical predictions, based solely on the ground state, tends to underestimate the experimental values. This discrepancy can be mitigated by incorporation contributions from excited states. We extended the theoretical analysis, including the contributions from the long-lived metastable states with lifetimes exceeding 1.5×10^{-5} s. We employed two statistical models to predict the fraction of ground state ions in the parent ion beam. Assuming a 79% fraction of parent ions in ground configuration, the experiment measurements align with the predictions. Furthermore we derived the theoretical cross-section for the ground state as correlated plasma rate coefficients, and compared it with existing data. Despite the uncertainty in our calculations, our results are still acceptable.

Keywords: tungsten ions, electron-impact ionization, cross section

PACS: 34.50.Fa, 34.80.Dp, 32.80.Aa **DOI:** 10.1088/1674-1056/ad1487

1. Introduction

Tungsten is utilized to coat sections of the inner walls in fusion devices due to its exceptional attributes, including a high melting point, resistance to neutron radiation, low tritium retention, and minimal chemical erosion.[1,2] When energetic particles bombard the inner walls, tungsten atoms are expelled and migrate towards the central regions of the thermonuclear plasma. During their journey from the wall regions to the plasma center, these tungsten atoms undergo multiple ionizations. The presence of tungsten ions in the plasma significantly contributes to radiative losses. Consequently, precise atomic data are indispensable for forecasting the impact of tungsten as a plasma impurity on plasma performance, encompassing atomic processes and the atomic structure of tungsten across all charged states.[3] Among the various ionization processes in fusion plasma, electron-impact single ionization (EISI) stands as the most dominant.[4,5] Therefore, comprehensive knowledge of ionization cross sections for tungsten ions, extending up to the highest charge states, is essential for fusion plasma modeling.

Over the years, investigations related to electron-impact ionization of tungsten have been conducted. Montague and Harrison[6] initially presented experimental cross sections for single ionization of W^+. These results were subsequently corroborated by Stenke *et al.*,[7] encompassing a range of W^{q+} (where $q = 1$–10). Additional, experimental cross sections were measured for W^{17+} and W^{19+} using an electron–ion crossed-beam setup.[4,8] Most recently, Schury *et al*. addressed the remaining gap for low to moderately high charge states with measurements for W^{q+} (where $11 \leq q \leq 18$).[9]

Theoretically, calculating electron-impact ionization (EII) cross sections for tungsten ions presents challenges due to its complex many-electron nature, relativistic effects, and the presence of open d or f shells. Consequently, several theoretical methods have been employed, including the widely used Lotz expression,[10] binary-encounter Bethe (BEB) model,[11,12] plane-wave Born (PWB) approximation,[13,14] *R*-matrix method,[15] and configuration-averaged distorted wave (CADW) method.[16] For instance, Kwon *et al*. calculated cross sections for the electron-impact ionization of neutral W atoms and W^+ ions using the BEB model and PWB approximation.[17] Balance *et al*. employed the distorted wave theory to calculate direct ionization (DI), while the relativistic *R*-matrix method was used to compute the excited autoionization (EA) contribution of W^{3+}.[18] The CADW method was employed to investigate electron-impact single ionization (EISI) for the ground state of all charged states of W ions.[16] Additionally, the level-to-level distorted wave (LLDW) method is widely applied in calculations, such as the investigation of EISI cross sections for W^{38+}–W^{45+} using the LLDW method.[5] Our research group conducted detailed theoretical calculations and investigations on the electron-impact ionization of W^{4+}, W^{5+}, and W^{17+} using the LLDW method, considering both direct ionization (DI) and excitation autoionization (EA) contributions.[2,19] Jonauskas *et al*. meticulously reevaluated the EISI cross section of W^{5+}, both through rigorous experimentation and comprehensive theoretical analy-

†Corresponding author. E-mail: zhangdh@nwnu.edu

© 2024 Chinese Physical Society and IOP Publishing Ltd

sis. They discovered that metastable states exert a pronounced influence on the overall ionization cross-section, particularly with regards to contributions stemming from the $5p^25d^2$ and $4f^{13}5d^2$ configurations. Remarkably, the agreement between theory and experiment was found to be excellent when assuming that approximately $85\% \pm 9\%$ of the parent ions are in the ground configuration.[20] Furthermore, detailed LLDW calculations for W^{7+}, W^{9+}, and W^{10+} have been presented by Chen *et al.*[21] and Bao *et al.*[22] placing particular emphasis on understanding the contribution of metastable states to the overall EISI cross section.

In collision experiments, the presence of metastable ions in the ion source is inevitable. Therefore, the measurement of W^{q+} ions is often influenced by numerous unknown metastable fractions. From the experimental data of W^{8+} ion, we have observed significant ionization signals below the ionization threshold for the ground state. As described by Stenke in the literature, these ionization signals manifest in the energy range of approximately 90 eV to 100 eV, precisely aligning with the ionization threshold for the excited state configuration involving 5p–5d excitation.[7] Furthermore Lu *et al.* have also reported the presence of characteristic spectral lines arising from configurations $4f^{13}5p^5$ and $4f^{12}5p^6$ when observing visible spectral lines of W^{8+} using an electron–beam ion trap apparatus.[23] Due to the nearly identical energy levels of the 4f and 5p electron orbitals for the W^{8+} ion, the calculations remain highly challenging. Previously, only Stenke predicted the electron-impact single ionization cross sections of the ground state $4f^{14}5p^4$ and the excited state $5p^35d$ of W^{8+} using the semiempirical Lotz formula. However, due to the influence of metastable states, the experimental results were severely underestimated. To comprehensively analyze the experimental data, we conducted a more detailed LLDW theoretical calculation for W^{8+} ion using the FAC code developed by Gu *et al.*[24] Additionally, we also accounted for contributions from metastable states.

2. Theoretical approach

The total ionization cross section for the main EISI process is given by

$$\sigma_{ij}(\varepsilon) = \sigma_{ij}^{\mathrm{DI}}(\varepsilon) + \sum_k \sigma_{ik}^{\mathrm{CE}}(\varepsilon) B_{kj}^a, \tag{1}$$

where ε is the energy of the incident electron, $\sigma_{ij}^{\mathrm{DI}}(\varepsilon)$ is the direct ionization cross section from level i of A^{q+} to level j of A^{q+1}, $\sigma_{ik}^{\mathrm{CE}}(\varepsilon)$ is the collisional excitation cross section from level i of A^{q+} to level k of A^{q+}, B_{kj}^a is the autoionization branching ratio from level k of A^{q+} to energy level j of A^{q+1}. The autoionization branching ratio can be expressed as

$$B_{kj}^a = \frac{A_{kj}^a}{\sum_m A_{km}^r + \sum_n A_{kn}^a}, \tag{2}$$

where A_{km}^r is the radiative decay rate of A^{q+} ion from level k of A^{q+} to level m of A^{q+}, and A_{kn}^a is the autoionization rate from level k of A^{q+} to energy level n of A^{q+1}.

When the incident electron energy is ε, the DI cross section is expressed as

$$\sigma_{ij}^{\mathrm{DI}}(\varepsilon) = \frac{1}{k_i^2 g_i} \Omega_{ij}. \tag{3}$$

The EA cross section is expressed as

$$\sigma_{ik}^{\mathrm{CE}}(\varepsilon) = \frac{\pi}{k_i^2 g_i} \Omega_{ik}, \tag{4}$$

where k_i is the kinetic momentum of the incident electron, g_i is the statistical weight of the initial state, and Ω_{ij}, Ω_{ik} are the collisional strength.

The experimental results indicate that the ionization cross section of W^{8+} includes a contribution from excited states. Hence, it is essential to calculate the total ionization cross section for both the ground state and the excited states. In order to fit the experimental cross section, it is necessary to estimate the different fractions of the ground state and excited states in the parent ion beam.

The experimental cross section can be expressed by

$$\sigma^{\mathrm{exp}}(\varepsilon) = \sum_{i=1}^{m} \lambda_i \sigma_i^{\mathrm{th}}(\varepsilon), \tag{5}$$

where λ_i is the ion–beam fraction of level i, m is the number of levels contributing to the measurements.[20]

3. Results and discussion

3.1. The ground state $4f^{14}5p^4$

3.1.1. Energy levels

Figure 1 shows the energy levels for the ground state of the W^{8+} ion, as well as select excited states. Additionally, energy levels of the main configurations for W^{9+} and W^{10+} ions produced by collisional ionization. The figure clearly illustrates that the energy levels of $5lnl'$ and $4fnl'$ either exceed or below the first ionization threshold, while the energy levels associated with the $4d^95p^47l'$ configuration span the second ionization threshold. In these cases, the configuration-averages approach may yield inaccurate results when considering contributions from these autoionization configurations to the total EISI cross sections. However, dealing with the EA cross section of excited configurations near the ionization threshold is more convenient for the LLDW method. It is important to mention that the energy levels of the 4d hole system lie above the second ionization threshold, resulting in net double ionization. Therefore, the 4d subshell only contributes to indirect processes.

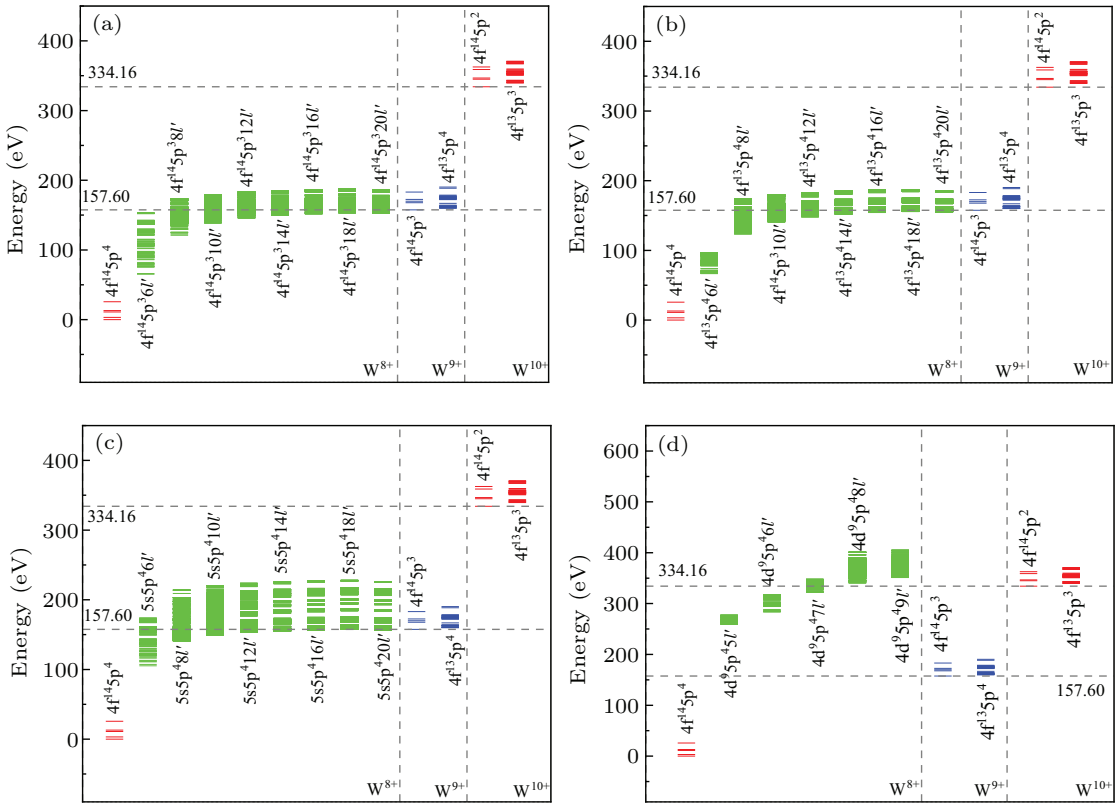


Fig. 1. The energy levels of W^{8+}, W^{9+}, and W^{10+} configurations considered in this paper. Where red indicates even configurations, blue indicates odd configurations, and green indicates part of excited state energy levels for 5p subshell (a), 4f subshell (b), 5s subshell (c), 4d subshell (d) electrons excited to $n \leq 20$, $l' \leq 6$.

3.1.2. Comparison of theoretical and experimental result

In Table 1, we present the ionization thresholds for the outer subshell electrons of both the ground state and the excited state $5p^35d$ configuration of the W^{8+} ion. Experimental results and NIST recommended values are included for comparison. Notably, the deviation between theoretical calculations and experimental results does not exceeds 1 eV.

Table 1. Threshold energies for the ionization of electrons in the outer subshells of W^{8+} ion ground state $4f^{14}5p^4$ and excited state $5p^35d$.

Configuration	Method	5d (eV)	4f (eV)	5p (eV)	5s (eV)	4d (eV)
$4f^{14}5p^4$	FAC		157.60	160.04	198.18	377.20
	Expt[a]		157.60	160.60	198.20	378.00
	NIST[b]		160.20 ± 1.20			
$4f^{14}5p^35d$	FAC	114.55	160.00	161.62	197.35	
	Expt[a]	114.50	160.00	160.00	196.80	

[a]Ref. [7], [b]Ref. [25].

Based on Fig. 1, the DI channel can be represented as follows:

$$\begin{aligned} &e^- + [Kr]4d^{10}5s^24f^{14}5p^4 \rightarrow \\ &[Kr]4d^{10}5s^24f^{14}5p^3 + 2e^-, \\ &[Kr]4d^{10}5s^24f^{13}5p^4 + 2e^-, \\ &[Kr]4d^{10}5s^14f^{13}5p^4 + 2e^-, \\ &[Kr]4d^{9}5s^24f^{14}5p^4 + 2e^-. \end{aligned} \tag{6}$$

According to Fig. 1, the EA contribution within the EISI of W^{8+} encompasses the 5p, 5s, 4f, and 4d subshells. These excitation channels can be expressed as

$$\begin{aligned} &e^- + [Kr]4d^{10}5s^24f^{14}5p^4 \rightarrow \\ &[Kr]4d^{10}5s^24f^{14}5p^3(d,f,g)^1 + e^-, \\ &[Kr]4d^{10}5s^24f^{13}5p^4(d,f,g)^1 + e^-, \\ &[Kr]4d^{10}5s4f^{14}5p^4(d,f,g)^1 + e^-, \\ &[Kr]4d^{9}5s^24f^{14}5p^4(d,f,g)^1 + e^-, \\ &[Kr]4d^{10}5s^24f^{14}5p^3nl' + e^-, \\ &[Kr]4d^{10}5s^24f^{13}5p^4nl' + e^-, \\ &[Kr]4d^{10}5s4f^{14}5p^4nl' + e^-, \\ &[Kr]4d^{9}5s^24f^{14}5p^4nl' + e^-, \\ &[Kr]4d^{10}5s4f^{14}5p^5 + e^-, \\ &[Kr]4d^{9}5s^24f^{14}5p^5 + e^-, \end{aligned} \tag{7}$$

where $5 \leq n \leq 20$, $l' \leq 6$, These excitation channels can be performed via autoionization (AI) or radiative (RT)

$$
\begin{aligned}
&\text{AI} \rightarrow \\
&[\text{Kr}]4\text{d}^{10}5\text{s}^2 5\text{p}^4 4\text{f}^{13} + \text{e}^-, \\
&[\text{Kr}]4\text{d}^{10}5\text{s}^2 5\text{p}^3 4\text{f}^{14} + \text{e}^-, \\
&[\text{Kr}]4\text{d}^{10}5\text{s}5\text{p}^4 4\text{f}^{14} + \text{e}^-, \\
&[\text{Kr}]4\text{d}^{9}5\text{s}^2 5\text{p}^4 4\text{f}^{14} + \text{e}^-, \\
&[\text{Kr}]4\text{d}^{9}5\text{s}^2 5\text{p}^5 4\text{f}^{13} + \text{e}^-, \\
&[\text{Kr}]4\text{d}^{10}5\text{s}^2 5\text{p}^5 4\text{f}^{12} + \text{e}^-, \\
&[\text{Kr}]4\text{d}^{10}5\text{s}5\text{p}^5 4\text{f}^{13} + \text{e}^-, \\
&[\text{Kr}]4\text{d}^{10}5\text{s}^2 5\text{p}^4 4\text{f}^{12} 5(\text{d},\text{f},\text{g})^1 + \text{e}^-, \\
&[\text{Kr}]4\text{d}^{10}5\text{s}^2 5\text{p}^3 4\text{f}^{13} 5(\text{d},\text{f},\text{g})^1 + \text{e}^-, \\
&[\text{Kr}]4\text{d}^{10}5\text{s}^2 5\text{p}^2 4\text{f}^{14} 5(\text{d},\text{f},\text{g})^1 + \text{e}^-, \\
&[\text{Kr}]4\text{d}^{10}5\text{s}5\text{p}^4 4\text{f}^{13} 5(\text{d},\text{f},\text{g})^1 + \text{e}^-, \\
&[\text{Kr}]4\text{d}^{10}5\text{s}5\text{p}^3 4\text{f}^{14} 5(\text{d},\text{f},\text{g})^1 + \text{e}^-, \\
&[\text{Kr}]4\text{d}^{10}5\text{p}^4 4\text{f}^{14} 5(\text{d},\text{f},\text{g})^1 + \text{e}^-, \\
&[\text{Kr}]4\text{d}^{10}5\text{s}^2 5\text{p}^4 4\text{f}^{12} nl' + \text{e}^-, \\
&[\text{Kr}]4\text{d}^{10}5\text{s}^2 5\text{p}^3 4\text{f}^{13} nl' + \text{e}^-, \\
&[\text{Kr}]4\text{d}^{10}5\text{s}^2 5\text{p}^2 4\text{f}^{14} nl' + \text{e}^-, \\
&[\text{Kr}]4\text{d}^{10}5\text{s}5\text{p}^4 4\text{f}^{13} nl' + \text{e}^-, \\
&[\text{Kr}]4\text{d}^{10}5\text{s}5\text{p}^3 4\text{f}^{14} nl' + \text{e}^-, \\
&[\text{Kr}]4\text{d}^{10}5\text{p}^4 4\text{f}^{14} nl' + \text{e}^-, \qquad (8) \\
&\text{RT} \rightarrow \\
&[\text{Kr}]4\text{d}^{9}5\text{s}^2 5\text{p}^5 4\text{f}^{14} + h\nu, \\
&[\text{Kr}]4\text{d}^{10}5\text{s}^2 5\text{p}^4 4\text{f}^{14} + h\nu, \\
&[\text{Kr}]4\text{d}^{9}5\text{s}^2 5\text{p}^6 4\text{f}^{13} + h\nu, \\
&[\text{Kr}]4\text{d}^{9}5\text{s}^2 5\text{p}^5 4\text{f}^{13} 5(\text{d},\text{f},\text{g})^1 + h\nu, \\
&[\text{Kr}]4\text{d}^{10}5\text{s}^2 5\text{p}^4 4\text{f}^{13} 5(\text{d},\text{f},\text{g})^1 + h\nu, \\
&[\text{Kr}]4\text{d}^{10}5\text{s}^2 5\text{p}^3 4\text{f}^{14} 5(\text{d},\text{f},\text{g})^1 + h\nu, \\
&[\text{Kr}]4\text{d}^{10}5\text{s}5\text{p}^4 4\text{f}^{14} 5(\text{d},\text{f},\text{g})^1 + h\nu, \\
&[\text{Kr}]4\text{d}^{9}5\text{s}^2 5\text{p}^5 4\text{f}^{13} nl' + h\nu, \\
&[\text{Kr}]4\text{d}^{10}5\text{s}^2 5\text{p}^4 4\text{f}^{13} nl' + h\nu, \\
&[\text{Kr}]4\text{d}^{10}5\text{s}^2 5\text{p}^3 4\text{f}^{14} nl' + h\nu, \\
&[\text{Kr}]4\text{d}^{10}5\text{s}5\text{p}^4 4\text{f}^{14} nl' + h\nu. \qquad (9)
\end{aligned}
$$

All energy levels within the 5s, 5p, and 4f hole system in DI are situated below the double ionization threshold. Figure 2 shows the contribution of the DI cross section originating from the 5p, 5s, and 4f subshells. It is evident that the primary contribution to the DI cross section arises from the 4f subshell, while the contribution of the 5p and 5s subshells decreases successively.

Regarding the contribution of nl' energy levels to the total cross section in the EA process of the ground state, we calculated the ratio of nl' to the total EA cross section at the peak energy (i.e., 377 eV). As shown in Fig. 3, the most significant contribution comes from excitations involving nl' $(n = 5)$. The nl' $(n = 20)$ level's accounts for approximately 1.3% of the total EA cross section. Contributions from higher nl' values beyond $20l'$ are expected to be even smaller. In this study, we have disregarded the contribution of the nl' $(n > 20)$ levels.

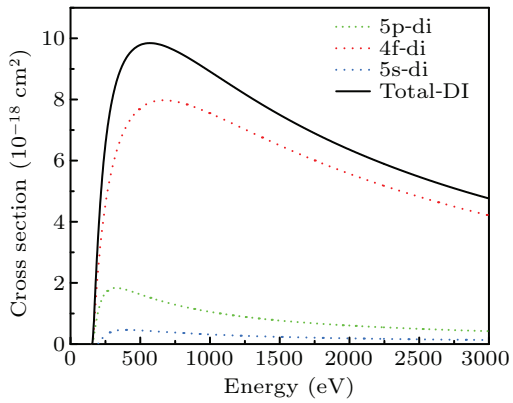


Fig. 2. Present calculated direct ionization (DI) cross sections for the W^{8+} ground state (contributions from different subshells).

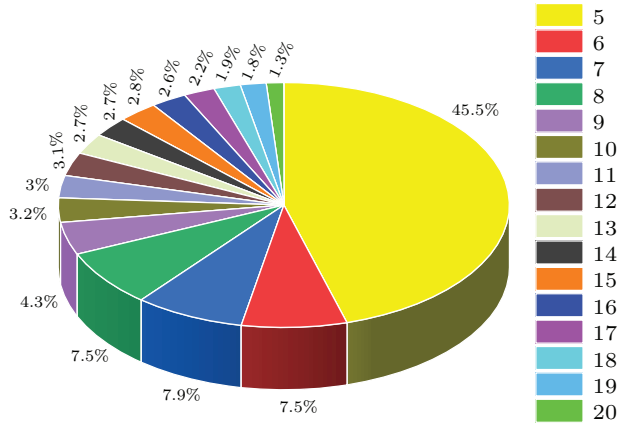


Fig. 3. The proportions of nl' $(n = 5$–$20)$ energy levels to the total cross section in EA processes of ground state $[\text{Cd}]4\text{f}^{14}5\text{p}^4$.

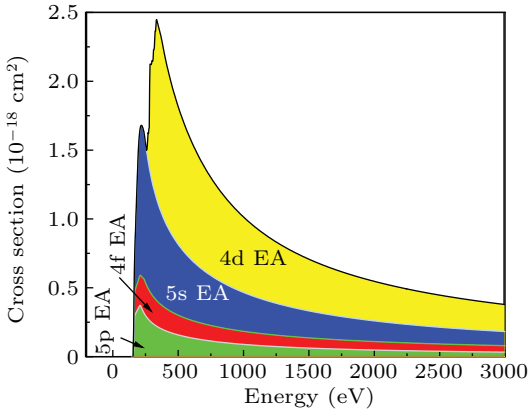


Fig. 4. Accumulated excitation autoionization (EA) cross sections (contributions from different subshells) for the W^{8+} ground state. The shadow areas show contributions from different subshells.

Figure 4 illustrates the contribution of nl' energy levels to the total cross section for EA, originating from the 5p, 5s, 4f, and 4d subshells. As observed in Fig. 1, energy levels in the 5p-nl' and 4f-nl' configurations rarely reach the first ionization threshold. Consequently, the contributions of the 5p and

4f subshells to the overall EA cross section are minimal. It is evident that the primary contribution to the EA cross section arises from the excited states of the 5s-nl' and 4d-nl' configurations.

Figure 5 presents a comparison between our computed cross section for the ground state of the W^{8+} ion and experimental results obtained by Stenke *et al.*[7] It is evident that the theoretical cross section of the ground state is 20% lower than the experimental measurement at the peak energy (i.e., 300 eV). Notably, the experimental measurements reveal a significant ionization signal occurring near 100 eV (while we have calculated an ionization potential of 157.6 eV), indicating that the ionization channel has been opened well below the ionization potential of the ground state.[7] Therefore, it is imperative to consider for the influence of metastable states on the ionization cross section of W^{8+}.

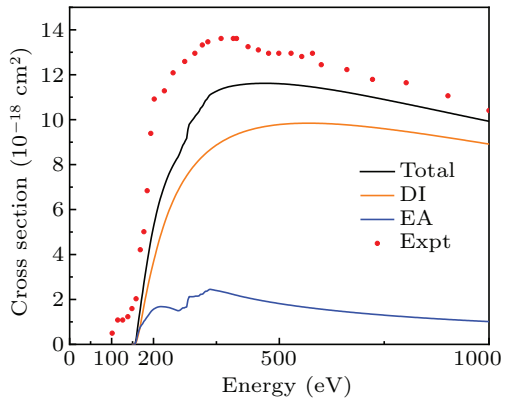


Fig. 5. Total direct ionization (DI) and excitation autoionization (EA) cross sections for the W^{8+} ground state, comparison of total EISI cross sections with the experimental results.

3.2. Theoretical modeling of metastable fraction

We have computed the total ionization cross sections for the long-lived energy levels associated with the configurations $4f^{14}5p^4$, $4f^{13}5p^5$, $4f^{12}5p^6$, and $4f^{14}5p^35d$. All possible E1, E2, E3, M1, and M2 transitions have been considered from these energy levels to determine their lifetimes. Based on previous research, we understand that the lifetime of excited ions generated by the ion source must exceed 1.5×10^{-5} s in order to reach the interaction region.[20]

Table 2 displays the lifetimes of specific energy levels within the aforementioned configurations $4f^{14}5p^4$, $4f^{13}5p^5$, $4f^{12}5p^6$, and $4f^{14}5p^35d$.

Referring to Table 2, the four energy levels of ground state [Cd]$4f^{14}5p^4$ (see Table 2 for the index i) have long lifetimes, their contributions to the total cross section should be considered, as shown in Fig. 6(a).

3.2.1. The metastable configuration [Cd]$4f^{13}5p^5$

The twelve energy levels of metastable [Cd]$4f^{13}5p^5$ (refer to Table 2 for index i) exhibit long lifetimes, necessitating their inclusion in the evaluation of the total cross section, as illustrated in Fig. 6(b). The DI channel can be expressed as

$$\begin{aligned}&e^- + [Pd]5s^24f^{13}5p^5 \rightarrow\\ &[Pd]5s^24f^{13}5p^4 + 2e^-,\\ &[Pd]5s^24f^{12}5p^5 + 2e^-,\\ &[Pd]5s4f^{13}5p^5 + 2e^-.\end{aligned} \tag{10}$$

Table 2. Long-lived levels of W^{8+} and associated lifetimes. Only levels with lifetime over 1.5×10^{-5} s are presented. Note that $a\pm b = a\times10^{\pm b}$.

Configuration	Index	Level	$2J$	Energy (eV)	Lifetime (s)
$4f^{14}5p^4$	0	$5p_+^25p_-^2$	4	0	–
	1	$5p_+^25p_-^2$	0	3.32	4.16×10^{-1}
	2	$5p_+^35p_-$	2	11.06	7.03×10^{-5}
	3	$5p_-5p_+^3$	4	12.99	1.10×10^{-4}
	4	$5p_+^4$	0	25.73	2.04×10^{-5}
$4f^{13}5p^5$	5	$4f_+^75p_+^3$	8	0.78	8.11×10^{3}
	6	$4f_+^75p_+^3$	6	0.87	8.17×10^{3}
	7	$4f_+^75p_+^3$	10	1.34	5.15
	8	$4f_+^55p_+^3$	6	2.78	1.14×10^{-2}
	9	$4f_+^75p_+^3$	4	2.92	5.49×10^{-3}
	10	$4f_-^55p_+^3$	4	3.59	8.77×10^{-4}
	11	$4f_-^55p_+^3$	8	4.42	4.24×10^{-3}
	12	$4f_-^55p_+^3$	2	4.67	2.34×10^{-2}
	13	$4f_+^75p_-^1$	6	13.71	5.75×10^{-5}
	14	$4f_+^75p_-^1$	8	14.07	5.43×10^{-5}
	15	$4f_-^55p_-^1$	6	15.44	5.93×10^{-5}
	16	$4f_-^55p_-^1$	4	16.61	5.09×10^{-5}
$4f^{12}5p^6$	17	$4f_+^6$	12	6.40	3.35×10^{-1}
	18	$4f_+^6$	8	7.41	1.41×10^{-1}
	19	$4f_-^54f_+^7$	10	8.51	7.47×10^{-3}
	20	$4f_-^54f_+^7$	8	9.39	1.72×10^{-2}
	21	$4f_+^6$	4	9.63	8.99×10^{-2}
	22	$4f_-^54f_+^7$	6	9.76	9.13×10^{-3}
	23	$4f_-^4$	8	11.33	4.35×10^{-3}
	24	$4f_-^54f_+^7$	4	12.38	4.54×10^{-3}
	25	$4f_-^54f_+^7$	12	13.45	7.83×10^{-3}
	26	$4f_+^6$	0	13.81	1.24×10^{-2}
	27	$4f_-^54f_+^7$	2	14.27	7.41×10^{-3}
	28	$4f_-^4$	4	14.77	3.38×10^{-3}
	29	$4f_-^4$	0	21.70	6.03×10^{-4}
$4f^{14}5p^35d$	30	$5p_+5d_+$	8	44.91	1.08×10^{-2}
	31	$5p_-5p_+^25d_+$	8	54.84	1.10×10^{-4}
	32	$5p_-5p_+^25d_-$	8	55.90	3.39×10^{-4}
	33	$5p_-5p_+^25d_+$	8	57.02	4.73×10^{-4}
	34	$5p_-5p_+^25d_+$	10	57.34	3.99×10^{-4}
	35	$5p_+^35d_+$	8	69.58	3.19×10^{-5}

The EA process includes excitations from the 5s, 5p, and 4f subshells of the metastable configuration. These excitations are graphically represented as

$$\begin{aligned}&e^- + [Pd]5s^24f^{13}5p^5 \rightarrow\\ &[Pd]5s^24f^{14}5p^4 + e^-,\\ &[Pd]5s4f^{14}5p^5 + e^-,\\ &[Pd]5s^24f^{12}5p^6 + e^-,\\ &[Pd]5s4f^{13}5p^6 + e^-,\\ &[Pd]5s^24f^{12}5p^55(d,f,g)^1 + e^-,\end{aligned}$$

$$
\begin{aligned}
&[\mathrm{Pd}]5s^2 4f^{13} 5p^4 5(d,f,g)^1 + e^-,\\
&[\mathrm{Pd}]5s 4f^{13} 5p^5 5(d,f,g)^1 + e^-,\\
&[\mathrm{Pd}]5s^2 4f^{12} 5p^5 nl' + e^-,\\
&[\mathrm{Pd}]5s^2 4f^{13} 5p^4 nl' + e^-,\\
&[\mathrm{Pd}]5s 4f^{13} 5p^5 nl' + e^-, \qquad (11)
\end{aligned}
$$

where $5 \le n \le 12$, $l' \le 6$, These excitation channels can be performed via autoionization (AI) or radiative (RT)

$$
\begin{aligned}
&\mathrm{AI} \rightarrow\\
&[\mathrm{Pd}]5s^2 5p^5 4f^{12} + e^-,\\
&[\mathrm{Pd}]5s^2 5p^4 4f^{13} + e^-,\\
&[\mathrm{Pd}]5s^2 5p^6 4f^{11} + e^-,\\
&[\mathrm{Pd}]5s^2 5p^3 4f^{14} + e^-,\\
&[\mathrm{Pd}]5s 5p^5 4f^{13} + e^-,\\
&[\mathrm{Pd}]5s 5p^6 4f^{12} + e^-,\\
&[\mathrm{Pd}]5s 5p^4 4f^{15} + e^-,\\
&[\mathrm{Pd}]5s^2 5p^5 4f^{11} 5(d,f,g)^1 + e^-,\\
&[\mathrm{Pd}]5s^2 5p^4 4f^{12} 5(d,f,g)^1 + e^-,\\
&[\mathrm{Pd}]5s^2 5p^3 4f^{13} 5(d,f,g)^1 + e^-,\\
&[\mathrm{Pd}]5s^2 5p^5 4f^{11} nl' + e^-,\\
&[\mathrm{Pd}]5s^2 5p^4 4f^{12} nl' + e^-,\\
&[\mathrm{Pd}]5s^2 5p^3 4f^{13} nl' + e^-, \qquad (12)\\
&\mathrm{RT} \rightarrow\\
&[\mathrm{Pd}]5s^2 5p^5 4f^{13} + h\nu,\\
&[\mathrm{Pd}]5s 5p^6 4f^{13} + h\nu,\\
&[\mathrm{Pd}]5s 5p^5 4f^{14} + h\nu,\\
&[\mathrm{Pd}]5s^2 5p^6 4f^{12} + h\nu,\\
&[\mathrm{Pd}]5s^2 5p^4 4f^{14} + h\nu,\\
&[\mathrm{Pd}]5s^2 5p^5 4f^{12} 5(d,f,g)^1 + h\nu,\\
&[\mathrm{Pd}]5s^2 5p^4 4f^{13} 5(d,f,g)^1 + h\nu,\\
&[\mathrm{Pd}]5s 5p^6 4f^{12} 5(d,f,g)^1 + h\nu,\\
&[\mathrm{Pd}]5s 5p^4 4f^{14} 5(d,f,g)^1 + h\nu,\\
&[\mathrm{Pd}]5s^2 5p^5 4f^{12} nl' + h\nu,\\
&[\mathrm{Pd}]5s^2 5p^4 4f^{13} nl' + h\nu,\\
&[\mathrm{Pd}]5s 5p^6 4f^{12} nl' + h\nu,\\
&[\mathrm{Pd}]5s 5p^4 4f^{14} nl' + h\nu. \qquad (13)
\end{aligned}
$$

3.2.2. The metastable configuration [Cd]4f^{12}5p^6

The thirteen energy levels of metastable [Cd]4f^{12}5p^6, indexed as i in Table 2, exhibit long lifetimes. It is important to take into account their contributions to the total cross-section, as depicted in Fig. 6(c). The DI channel can be expressed as

$$
\begin{aligned}
&e^- + [\mathrm{Pd}]5s^2 4f^{12} 5p^6 \rightarrow\\
&[\mathrm{Pd}]5s^2 4f^{12} 5p^5 + 2e^-,\\
&[\mathrm{Pd}]5s^2 4f^{11} 5p^6 + 2e^-,\\
&[\mathrm{Pd}]5s 4f^{12} 5p^6 + 2e^-. \qquad (14)
\end{aligned}
$$

The EA process includes excitations from the 5s, 5p, and 4f subshells of the metastable configuration. These excitations are graphically represented as

$$
\begin{aligned}
&e^- + [\mathrm{Pd}]5s^2 4f^{12} 5p^6 \rightarrow\\
&[\mathrm{Pd}]5s^2 4f^{13} 5p^5 + e^-,\\
&[\mathrm{Pd}]5s 4f^{13} 5p^6 + e^-,\\
&[\mathrm{Pd}]5s^2 4f^{12} 5p^5 5(d,f,g)^1 + e^-,\\
&[\mathrm{Pd}]5s^2 4f^{11} 5p^6 5(d,f,g)^1 + e^-,\\
&[\mathrm{Pd}]5s 4f^{12} 5p^6 5(d,f,g)^1 + e^-,\\
&[\mathrm{Pd}]5s^2 4f^{12} 5p^5 nl' + e^-,\\
&[\mathrm{Pd}]5s^2 4f^{11} 5p^6 nl' + e^-,\\
&[\mathrm{Pd}]5s 4f^{12} 5p^6 nl' + e^-, \qquad (15)
\end{aligned}
$$

where $5 \le n \le 12$, $l' \le 6$, These excitation channels can be performed via autoionization (AI) or radiative (RT)

$$
\begin{aligned}
&\mathrm{AI} \rightarrow\\
&[\mathrm{Pd}]5s^2 5p^6 4f^{11} + e^-,\\
&[\mathrm{Pd}]5s^2 5p^5 4f^{12} + e^-,\\
&[\mathrm{Pd}]5s^2 5p^4 4f^{13} + e^-,\\
&[\mathrm{Pd}]5s 5p^5 4f^{13} + e^-,\\
&[\mathrm{Pd}]5s 5p^6 4f^{12} + e^-,\\
&[\mathrm{Pd}]5s^2 5p^6 4f^{10} 5(d,f,g)^1 + e^-,\\
&[\mathrm{Pd}]5s^2 5p^4 4f^{12} 5(d,f,g)^1 + e^-,\\
&[\mathrm{Pd}]5s^2 5p^5 4f^{11} 5(d,f,g)^1 + e^-,\\
&[\mathrm{Pd}]5s^2 5p^6 4f^{10} nl' + e^-,\\
&[\mathrm{Pd}]5s^2 5p^4 4f^{12} nl' + e^-,\\
&[\mathrm{Pd}]5s^2 5p^5 4f^{11} nl' + e^-, \qquad (16)\\
&\mathrm{RT} \rightarrow\\
&[\mathrm{Pd}]5s^2 5p^6 4f^{12} + h\nu,\\
&[\mathrm{Pd}]5s^2 5p^5 4f^{13} + h\nu,\\
&[\mathrm{Pd}]5s 5p^6 4f^{13} + h\nu,\\
&[\mathrm{Pd}]5s 5p^5 4f^{14} + h\nu,\\
&[\mathrm{Pd}]5s^2 5p^6 4f^{11} 5(d,f,g)^1 + h\nu,\\
&[\mathrm{Pd}]5s^2 5p^5 4f^{12} 5(d,f,g)^1 + h\nu,\\
&[\mathrm{Pd}]5s 5p^5 4f^{13} 5(d,f,g)^1 + h\nu,\\
&[\mathrm{Pd}]5s^2 5p^6 4f^{11} nl' + h\nu,\\
&[\mathrm{Pd}]5s^2 5p^5 4f^{12} nl' + h\nu,\\
&[\mathrm{Pd}]5s 5p^5 4f^{13} nl' + h\nu. \qquad (17)
\end{aligned}
$$

3.2.3. The metastable configuration [Cd]4f^{14}5p^{3}5d

The six energy levels of metastable [Cd]4f^{14}5p^{3}5d (refer to Table 2 for index i) exhibit long lifetimes. It is important to

take into account their contributions to the total cross-section, as depicted in Fig. 6(d). The DI channel can be expressed as

$$\begin{aligned}&e^- + [Pd]5s^24f^{14}5p^35d \rightarrow\\ &[Pd]5s^24f^{14}5p^3 + 2e^-,\\ &[Pd]5s^24f^{14}5p^25d + 2e^-,\\ &[Pd]5s^24f^{13}5p^35d + 2e^-,\\ &[Pd]5s4f^{14}5p^35d + 2e^-.\end{aligned} \tag{18}$$

The EA process includes excitations from the 5s, 5p, and 4f subshells of the ground configuration. These excitations are graphically represented as

$$\begin{aligned}&e^- + [Pd]5s^24f^{14}5p^35d \rightarrow\\ &[Pd]5s^24f^{13}5p^45d + e^-,\\ &[Pd]5s4f^{14}5p^45d + e^-,\\ &[Pd]5s^24f^{14}5p^25d^2 + e^-,\\ &[Pd]5s^24f^{13}5p^35d^2 + e^-,\\ &[Pd]5s4f^{14}5p^35d^2 + e^-,\\ &[Pd]5s^24f^{14}5p^35(f,g)^1 + e^-,\\ &[Pd]5s^24f^{14}5p^25d5(f,g)^1 + e^-,\\ &[Pd]5s^24f^{13}5p^35d5(f,g)^1 + e^-,\\ &[Pd]5s4f^{14}5p^35d5(f,g)^1 + e^-,\\ &[Pd]5s^24f^{14}5p^3nl' + e^-,\\ &[Pd]5s^24f^{14}5p^25dnl' + e^-,\\ &[Pd]5s^24f^{13}5p^35dnl' + e^-,\\ &[Pd]5s4f^{14}5p^35dnl' + e^-,\end{aligned} \tag{19}$$

where $5 \le n \le 12$, $l' \le 6$, These excitation channels can be performed via autoionization (AI) or radiative (RT)

$$\begin{aligned}&AI \rightarrow\\ &[Pd]5s^24f^{13}5p^4 + e^-,\\ &[Pd]5s^24f^{14}5p^3 + e^-,\\ &[Pd]5s4f^{14}5p^4 + e^-,\\ &[Pd]5s^24f^{12}5p^45d + e^-,\\ &[Pd]5s^24f^{13}5p^35d + e^-,\\ &[Pd]5s^24f^{12}5p^45d + e^-,\\ &[Pd]5s4f^{14}5p^35d + e^-,\\ &[Pd]5s4f^{13}5p^45d + e^-,\\ &[Pd]5s^24f^{12}5p^35d^2 + e^-,\\ &[Pd]5s^24f^{13}5p^25d^2 + e^-,\\ &[Pd]5s^24f^{14}5p^15d^2 + e^-,\\ &[Pd]5s^24f^{13}5p^35(f,g)^1 + e^-,\\ &[Pd]5s^24f^{14}5p^25(f,g)^1 + e^-,\\ &[Pd]5s4f^{14}5p^35(f,g)^1 + e^-,\\ &[Pd]5s^24f^{12}5p^35d5(f,g)^1 + e^-,\\ &[Pd]5s^24f^{13}5p^25d5(f,g)^1 + e^-,\\ &[Pd]5s^24f^{14}5p5d5(f,g)^1 + e^-,\\ &[Pd]5s4f^{13}5p^35d5(f,g)^1 + e^-,\\ &[Pd]5s4f^{14}5p^25d5(f,g)^1 + e^-,\\ &[Pd]5s^24f^{13}5p^3nl' + e^-,\\ &[Pd]5s^24f^{14}5p^2nl' + e^-,\\ &[Pd]5s4f^{14}5p^3nl' + e^-,\\ &[Pd]5s^24f^{12}5p^35dnl' + e^-,\\ &[Pd]5s^24f^{13}5p^25dnl' + e^-,\\ &[Pd]5s^24f^{14}5p5dnl' + e^-,\\ &[Pd]5s4f^{13}5p^35dnl' + e^-,\\ &[Pd]5s4f^{14}5p^25dnl' + e^-,\end{aligned} \tag{20}$$

$$\begin{aligned}&RT \rightarrow\\ &[Pd]5s4f^{14}5p^5 + h\nu,\\ &[Pd]5s^24f^{14}5p^4 + h\nu,\\ &[Pd]5s^24f^{14}5p^35d + h\nu,\\ &[Pd]5s4f^{13}5p^55d + h\nu,\\ &[Pd]5s^24f^{13}5p^45d + h\nu,\\ &[Pd]5s^24f^{14}5p^35d + h\nu,\\ &[Pd]5s4f^{14}5p^45d + h\nu,\\ &[Pd]5s4f^{13}5p^45d^2 + h\nu,\\ &[Pd]5s4f^{14}5p^35d^2 + h\nu,\\ &[Pd]5s^24f^{14}5p^25d^2 + h\nu,\\ &[Pd]5s^24f^{13}5p^35d^2 + h\nu,\\ &[Pd]5s^24f^{14}5p^35(f,g)^1 + h\nu,\\ &[Pd]5s4f^{14}5p^45(f,g)^1 + h\nu,\\ &[Pd]5s4f^{13}5p^45d5(f,g)^1 + h\nu,\\ &[Pd]5s^24f^{13}5p^35d5(f,g)^1 + h\nu,\\ &[Pd]5s^24f^{14}5p^3nl' + h\nu,\\ &[Pd]5s4f^{14}5p^4nl' + h\nu,\\ &[Pd]5s4f^{13}5p^45dnl' + h\nu,\\ &[Pd]5s^24f^{13}5p^35dnl' + h\nu.\end{aligned} \tag{21}$$

In order to analyze the distribution of metastable energy levels, it is necessary to assess the fraction λ_i (index i, see Table 2) of all possible energy levels. Due to the unavailability of this information from experimental data, Jonauskas introduced two models to fit the experimental data, and their validity has also been confirmed through calculations of W^{q+} ($q = 5, 9, 10$).[20,22]

In the first model, a statistical weight was assigned to each contributing configuration

$$\sigma^{\exp}(E_e) = \sum_k c_k \frac{\sum_i (2 \times {}^kJ_i + 1) \times {}^k\sigma_i^{\text{th}}(E_e)}{\sum_i (2 \times {}^kJ_i + 1)}, \tag{22}$$

where c_k is the fitting coefficient, ${}^kJ_i$ is the total angular momentum for the energy level i of configuration k, and ${}^k\sigma_i^{\rm th}(E_{\rm e})$ is the EISI cross section of energy level i in configuration k.

In the second model, it assumes that the excitation levels satisfy the Boltzmann distribution

$$\sigma^{\rm exp}(E_{\rm e}) = \sum_k c_k \frac{\sum_i (2\times {}^kJ_i+1)\exp[-E_i/(kT)]\times {}^k\sigma_i^{\rm th}(E_{\rm e})}{\sum_i (2\times {}^kJ_i+1)\exp[-E_i/(kT)}, \tag{23}$$

where c_k is the fitting coefficient, ${}^kJ_i$ is the total angular momentum for the energy level i of configuration k and ${}^k\sigma_i^{\rm th}(E_{\rm e})$ is the EISI cross section of energy level i in configuration k. T is the temperature of peak tungsten ion abundance, $T = 5.14\times 10^5$ K for W^{8+}.[26]

In this work, EISI cross sections have been computed for both the long-lived levels of the ground state ($4f^{14}5p^4$) and the excited states ($4f^{13}5p^5$, $4f^{12}5p^6$, and $4f^{14}5p^35d$). From Fig. 6, it is evident that under the same configuration, as the energy level index i (see Table 2) increases, the ionization threshold for each energy level gradually decreases, and the ionization cross section correspondingly increases. Compared to the ground state $4f^{14}5p^4$, the cross sections for excited states $4f^{13}5p^5$ and $4f^{12}5p^6$ are smaller than that of the ground state, but the cross section for excited state $4f^{14}5p^35d$ is greater than that of the ground state.

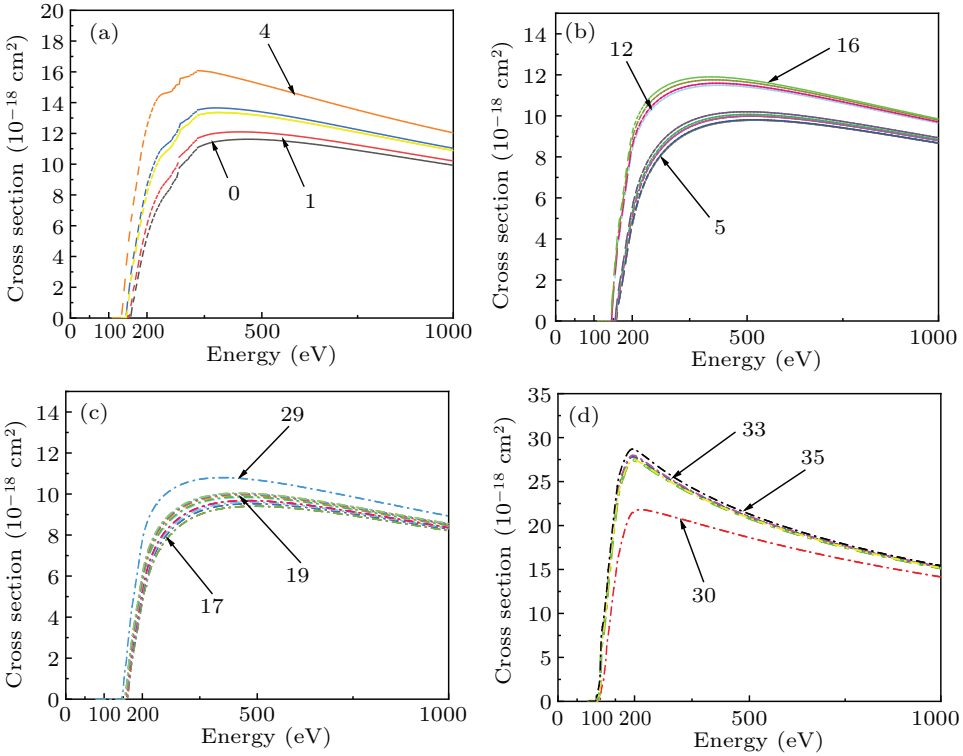


Fig. 6. Cross sections for the long-lived levels of the ground state $4f^{14}5p^4$ (a) and the excited states $4f^{13}5p^5$ (b), $4f^{12}5p^6$ (c), and $4f^{14}5p^35d$ (d) long-lived energy levels. Few selected cross sections are labeled by their index given in Table 2.

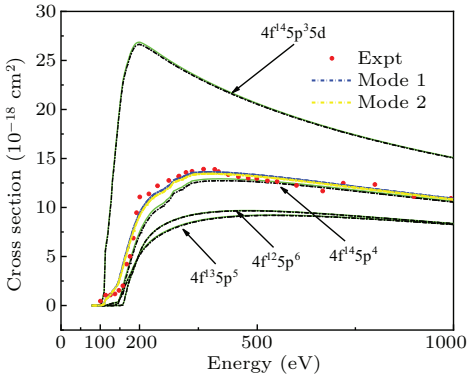


Fig. 7. Electron-impact ionization cross sections for the W^{8+} ion ground state, blue dashed line: the result for model 1, yellow dashed line: the result for model 2, red dotted line: the experimental results of Stenke *et al.*,[7] green solid line and the black dashed line respectively represent the results obtained by fitting configurations $4f^{14}5p^4$, $4f^{13}5p^5$, $4f^{12}5p^6$, and $4f^{14}5p^35d$ using two different models.

The comparison between the model cross sections and experimental data is shown in Fig. 7. The blue dashed line represents the results of model 1, while the yellow dashed line represents the results of model 2. The corresponding fractions of ions in the relevant configurations are 79% for the ground state $4f^{14}5p^4$, 5% for $4f^{13}5p^5$, 5% for $4f^{12}5p^6$, and 11% for $4f^{14}5p^35d$. It can be observed that the differences between the two models are very minor, and the fitted results align more closely with the experimental data.

3.3. Plasma rate coefficients

In order to facilitate modeling of thermonuclear fusion plasmas, we have generated plasma rate coefficients (PRCs) from our calculated EISI cross section for the W^{8+} ion ground state. The rate coefficient $\alpha_{ij}(T_{\rm e})$ for Maxwell–Boltzmann dis-

tribution at an electron temperature T_e is given by

$$\alpha_{ij}(T_e) = \left(\frac{1}{k_B T_e}\right)^{3/2}\left(\frac{8}{m_e \pi}\right)^{1/2} \times \int_0^{\infty} \varepsilon \sigma_{ij}(\varepsilon) \exp\left(-\frac{\varepsilon}{k_B T_e}\right) \mathrm{d}\varepsilon. \quad (24)$$

Here k_B is the Boltzmann constant, m_e is the electron mass, and $\sigma_{ij}(\varepsilon)$ is the cross section for the transition from the level i to the level j.

Figure 8 illustrates the PRCs of the W^{8+} ion transitioning from the ground state level i to all ionization final state levels j, alongside previously reported data calculated by the FLYCHK code.[27] It is evident that the electronic temperature ranges from 0 K to 1.16×10^7 K, with the results in the previous data slightly higher than our calculations. As the electronic temperature continues to rise, our calculated PRCs surpass existing results; however, our results exhibit a more pronounced decreasing trend. Therefore, after reaching 5.22×10^7 K, the PRCs from our calculations once again fall below their values. Nonetheless, the currently available PRCs data show minimal distinctions from one another. The reason for this difference may be attributed to variations in calculation methods, and unfortunately, we are unable to obtain further calculation-related information from the database. Considering the uncertainty in calculations, our results are still considered acceptable.

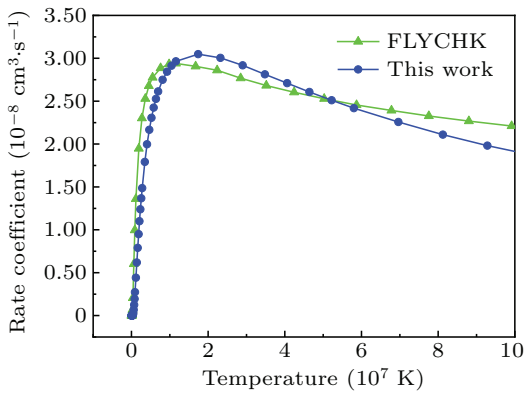


Fig. 8. Present plasma rate coefficients for electron-impact single ionization of W^{8+} ions in the ground state (circle solid line). The triangle solid line represent the data calculated by the FLYCHK code.[27]

4. Summary and discussion

The EISI cross section for the ground state of the W^{8+} ion was calculated using the level to level distorted-wave method implemented in the FAC code. The experimental results revealed a nonzero ionization signal below the ionization potential for the ground state $4f^{14}5p^4$, clearly indicating the presence of excited state ions in the parent ion beam. In order to estimate the metastable fractions, it was necessary to calculate the cross sections for all possible energy levels. Therefore theoretical cross sections were calculated for both the levels of the W^{8+} ground configuration $4f^{14}5p^4$ and the excited configurations $4f^{13}5p^5$, $4f^{12}5p^6$, and $4f^{14}5p^35d$, all with lifetimes exceeding 1.5×10^{-5} s. Assuming a 79% fraction of parent ions in ground configuration, the previous experimental measurements can be well reproduced. Additionally we derived the theoretical cross-section for the ground state as correlated plasma rate coefficients and compared it with existing data. It is reasonable to expect slight differences within the uncertainty range.

Acknowledgements

Project supported by the National Natural Science Foundation of China (Grant No. 12364034), the National Key Research and Development Program of China (Grant No. 2022YFA1602501), and the Science and Technology Project of Gansu Province, China (Grant No.23YFFA0074).

References

[1] Kynienė A, Merkelis G, Šukys A, Masys C, Pakalka S, Kisielius R and Jonauskas V 2018 *J. Phys. B: At. Mol. Opt. Phys.* **51** 155202
[2] Zhang D, Xie L, Jiang J, Wu Z, Dong C, Shi Y and Qu Y 2018 *Chin. Phys. B* **27** 053402
[3] Jin F, Borovik A, Ebinger B and Schippers S 2020 *J. Phys. B: At. Mol. Opt Phys.* **53** 075201
[4] Borovik A, Ebinger B, Schury D, Schippers S and Müller A 2016 *Phys. Rev. A* **93** 012708
[5] Bao R, Wei J, Li B and Chen X 2022 *Atoms* **10** 92
[6] Montague R G and Harrison M F A 1984 *J. Phys. B: At. Mol. Opt Phys.* **17** 2707
[7] Stenke M, Aichele K, Harthiramani D, Hofmann G, Steidl M, Volpel R and Salzborn E 1995 *J. Phys. B: At. Mol. Opt Phys.* **28** 2711
[8] Rausch J, Becker A, Spruck K, Hellhund J, Borovik A, Huber K, Schippers S and Müller A 2011 *J. Phys. B: At. Mol. Opt Phys.* **44** 165202
[9] Schury D, Borovik A, Ebinger B, Jin F, Spruck K, Müller A and Schippers S 2019 *J. Phys. B: At. Mol. Opt Phys.* **53** 015201
[10] Lotz W 1968 *Z. Physik* **216** 241
[11] Kim Y K and Rudd M E 1994 *Phys. Rev. A* **50** 3954
[12] Kim Y K, Migdałek J, Siegel W and Bieron J 1998 *Phys. Rev. A* **57** 246
[13] Bartlett P L and Stelbovics A T 2004 *Atomic Data and Nuclear Data Tables* **86** 235
[14] Omidvar K, Kyle H L and Sullivan E C 1972 *Phys. Rev. A* **5** 1174
[15] Scott N S and Burke P G 1980 *J. Phys. B: At. Mol. Opt Phys.* **13** 4299
[16] Loch S D, Ludlow J A, Pindzola M S, Whiteford A D and Griffin D C 2005 *Phys. Rev. A* **72** 052716
[17] Kwon D H, Rhee Y J and Kim Y K 2006 *International Journal of Mass Spectrometry* **252** 213
[18] Ballance C P, Loch S D, Pindzola M S and Griffin D C 2013 . *Phys. B: At. Mol. Opt Phys.* **46** 055202
[19] Zhang D H and Kwon D H 2014 *J. Phys. B: At. Mol. Opt Phys.* **47** 075202
[20] Jonauskas V, Kynienė A, Kučas S, Pakalka S, Masys I C V, Prancikevičius A, Borovik A, Gharaibeh M F, Schippers S and Müller A 2019 *Phys. Rev. A* **100** 062701
[21] Chen L, Li B and Chen X 2022 *Journal of Quantitative Spectroscopy and Radiative Transfer* **285** 108179
[22] Bao R, Wei J, Chen L, Li B and Chen X 2023 *Chin. Phys. B* **32** 063401
[23] Lu Q, Yan C L, Meng J, Xu G Q, Yang Y, Chen C Y, Xiao J, Li J G, Wang J G and Zou Y 2021 *Phys. Rev. A* **103** 022808
[24] Mingfeng G 2004 *AIP Conference Proceedings* 730 ISSN 0094-243X
[25] Kramida A, Ralchenko Yu, Reader J and NIST ASD Team 2023
[26] Preval S P, Badnell N R and O'Mullane M G 2018 *J. Phys. B: At. Mol. Opt. Phys.* **52** 025201
[27] Chung H K, Chen M, Morgan W, Ralchenko Y and Lee R 2005 *High Energy Density Physics* **1** 3